Strip waves in vibrated shear-thickening wormlike micellar solutions

T. Epstein and R. D. Deegan*
Department of Physics and the Center for the Study of Complex Systems, University of Michigan, Ann Arbor, Michigan 48109, USA
(Received 22 November 2009; published 21 June 2010)

We present an instability in vertically vibrated dilute wormlike micellar solutions. Above a critical driving acceleration the fluid forms elongated solitary domains of high amplitude waves. We model this instability using a Mathieu equation modified to account for the non-Newtonian character of the fluid. We find that our model successfully reproduces the observed transitions.

DOI: 10.1103/PhysRevE.81.066310 PACS number(s): 47.20.Gv, 47.20.Ma, 47.50.Gj, 47.54.−r

I. INTRODUCTION

Faraday [1] discovered that a vertically oscillated fluid spontaneously develops free surface waves. Over the past several decades, the Faraday system has become one of the canonical systems in which to study self-organization, and Faraday waves in Newtonian fluids have been extensively researched. Faraday envisioned a different application for his system: *The difference between oil and the white of egg is remarkable…the crispated state may be a useful and even important indication of the internal constitution of different liquids*. Faraday's vision is now being realized as his system is increasingly employed to study the rheology of complex fluids in temporal and spatial scales that are inaccessible through other techniques.

Starting with Wagner's [2] and Raynal's [3] investigations of polymeric solutions, the Faraday system is now commonly used to study complex fluids. Lioubashevski *et al.* [4] found localized traveling waves in shear-thinning clay suspensions, and were able to deduce the viscosity of the liquid from the threshold for Faraday waves. Localized structures were also observed by Merkt *et al.* [5] in a shear-thickening particulate suspension. Ballesta *et al.* examined dilute [6,7] and semidilute [8] wormlike micellar solutions in the Faraday system; in the semidilute regime they discovered a signature of the fluid's elasticity in the shape of the phase diagram boundary between the flat and wavy state, and in the dilute regime they observed the formation of shear-induced-structures driven by Faraday waves. Convection rolls induced by vibrations were observed by Shiba *et al.* [9] in a viscoplastic fluid, and by Ebata *et al.* [10] in non-Brownian suspensions.

Here we present the results of our study of a dilute wormlike micellar solution (WMS) in the Faraday system. Wormlike micellar solutions form in an aqueous solution of surfactant and salt. Surfactant molecules in water usually form spherical micelles; the addition of salt produces long polymerlike micelles as the salt is sequestered from the solution by the surfactant. The properties of these fluids are summarized in a recent review [11]. For our study, the most salient rheological characteristics of dilute WMS are that their response is purely viscous, their viscosity is shear-rate dependent, and they achieve their ultimate viscosity only after being sheared for a period called the induction time. The nonlinear rheological response of these fluids is considered to arise from flow induced mesoscopic structure [12].

Our system displays the usual Faraday waves above a critical acceleration, but additionally at a yet higher acceleration threshold a transition occurs in which the fluid accumulates into elongated domains of steep standing waves [see Fig. 1 and 2(b)]. We call these *strip waves*. Below we present our experimental characterization of this phenomenon and using a model for Faraday waves adapted for shear-rate dependent viscosity show that the rheological properties of the fluid are responsible for the formation of strip waves.

II. EXPERIMENTS

In our experiments we used worm-like micellar solutions made from an equimolar solution of cetyltrimethylammonium bromide (CTAB) and sodium salicylate (NaSal) with

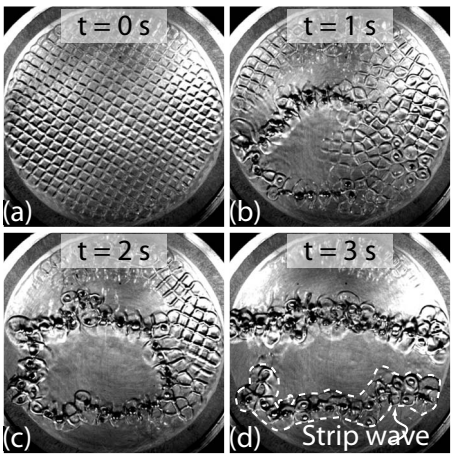

FIG. 1. Time evolution of the strip wave instability for $a=14$ g, $f=80$ Hz, $h=0.75$ mm, and $C=4$ mM. (a)–(d) Show the progression of the instability as viewed from directly above following an increase of the acceleration to the critical acceleration for the onset of strip waves. Immediately after the acceleration change the surface waves remain in the form of a square Faraday pattern corresponding to the preincrease value of the acceleration. Over the course of four seconds, the square pattern is destroyed by the nucleation and saturation of large amplitude waves that ultimately draw in all the fluid in the container. The boundary of a strip wave is shown in (d) by a dashed line.

*rddeegan@umich.edu

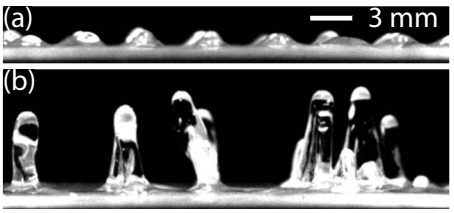

FIG. 2. Side view of surface waves (a) below and (b) above the critical acceleration for strip waves for $f=80$ Hz, $h=0.75$ mm, and $C=4$ mM. (a) Faraday waves at $a=7$ g. The peak-to-peak amplitude of the waves is 0.8 mm. (b) Fully developed strip waves at $a=13$ g. The peak-to-peak amplitude of the waves is 6.6 mm. Note that the amplitude of strip waves is eight times greater than Faraday waves.

concentrations for each components ranging from 0.5 to 10 mM. We measured the viscosity of our samples in a cone-plate geometry (40 mm radius, angle 2° solvent trap) using a AR2000ex (TA Instruments) rheometer at 25.0°. We followed the protocol of Hu *et al.* [13]. Each measurement was performed on a freshly loaded sample. The sample was allowed to thermally equilibrate with the instrument, after which a constant shear rate was applied. The stress either decreased or increased monotonically for the first 10–200 s, depending on the shear rate. After this transient period the stress reached a steady-state value about which it fluctuated. The average steady-state value of viscosity versus shear rate is plotted in Fig. 3. The error bars reflect the low and high values of the fluctuations about the average value. These data show the characteristic shear-rate dependence of the viscosity of dilute WMS: for shear rates $\dot{\gamma}$ below 10 s^{-1}, the viscosity decreases with shear rate; for intermediate shear rates $8\ s^{-1}<\dot{\gamma}<20\ s^{-1}$, the viscosity increases; and for high shear rates, the viscosity decreases. We designate these regimes shear-thinning I, shear-thickening, and shear-thinning II, respectively.

We vertically vibrated the solutions in a circular container mounted on an electrodynamic shaker (Labworks ET-140).

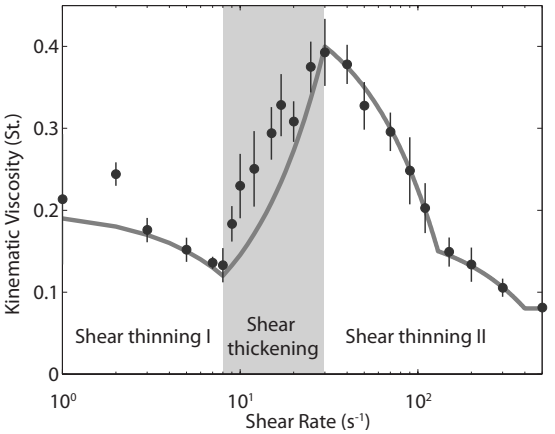

FIG. 3. Kinematic viscosity versus shear rate for a 4 mM CTAB/NaSal equimolar solution. Solid line denotes piecewise linear segment parameterization of viscosity given by ν_1 in Table I. The error bars represent fluctuations in the viscosity during a single measurement.

The temperature of the fluid was unregulated; periodic checks with a thermocouple showed no significant deviations from room temperature which fluctuated by ± 2 °C. Heating of the container due to the shaker was avoided by coupling the container to the shaker with an acrylic rod and by limiting the duration of the experiments.

In our initial experiments the container consisted of an aluminum plate and rigid Plexiglas sidewalls, but we found that the fluid agglomerated at the walls during vibration so that all the fluid ended up in a 1 cm band next to the wall. In order to avoid this boundary effect, we removed the walls and applied a thin coat of silicone glue to the perimeter of the plate. The solution was thus kept in the cell by the hydrophobicity of the boundary. We varied the depth of the fluid from 0.5 up to 2 mm. Layers shallower than 0.5 mm did not coat the substrate uniformly, and layers deeper than 2 mm escaped over hydrophobic coating. The cell was oscillated with acceleration $a(t)=a_o \cos(2\pi ft)$ where a_o is the peak acceleration and f is the driving frequency. We varied the acceleration from 0 to 40 g, where g is the acceleration due to gravity, and the frequency from 50 to 190 Hz. The acceleration was measured using an accelerometer (PCB 352c65) mounted on the shaker platform, and monitored with an oscilloscope. Our images were recorded with a high speed camera (Phantom 7.3, Vision Research) from either the top or side.

We observed the onset of square-pattern Faraday waves at low accelerations. The same pattern is universally observed in Newtonian fluids. However, unlike in Newtonian fluids or the semidilute WMS studied by Ballesta *et al.* [8], the Faraday waves for our dilute WMS were of finite amplitude at onset. Increasing the acceleration above onset produced waves of progressively, but modestly, larger amplitude until a second threshold was reached. At this second transition point we observed an instability which culminated in the fluid distributed into long and narrow domains of large amplitude waves [see Fig. 1(b)] separated by thin (<100 μm) layers of quiescent fluid. The instability manifested immediately upon reaching the transition point and the elongated structures reached saturation within a few seconds, with saturation occurring faster for lower frequencies. The boundaries of the domains were dynamic and shifted with time. As shown in Fig. 2, the wave amplitude increased by an order of magnitude after the transition to strip waves. Furthermore, we noted that despite their slender aspect ratio there was no tendency for the wave crests to pinch off into droplets as would be expected for a Newtonian fluid.

Strip waves occurred over the entire range of experimental accessible driving frequencies. Figures 4 and 5 show that the acceleration threshold increased with driving frequency, and depended weakly on the fluid depth and concentration. We also found depth and concentration thresholds beyond which the instability was absent. These thresholds are denoted in Fig. 5 by the absence of data for concentrations below 1 mM and for depths above a frequency-dependent value.

III. MODEL

We hypothesized that the strip wave instability is due to the drop in the viscosity when the shear rate generated by the

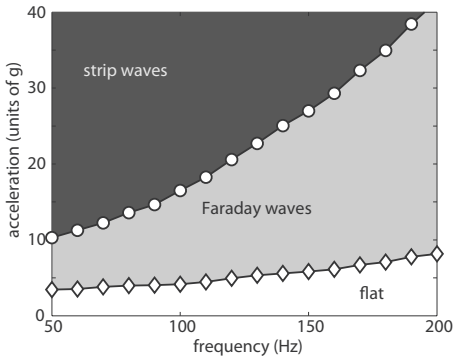

FIG. 4. Phase diagram of the instability as function of acceleration and frequency for $h=0.75$ mm and $C=4$ mM. The threshold acceleration for the transition from a flat interface to Faraday waves and from Faraday waves to strip waves are denoted by diamonds and circles, respectively.

Faraday waves exceeds the shear rate at the boundary between the shear-thickening and shear-thinning II regimes (see Fig. 3). Our reasoning was based on two well-known features of Faraday waves. First, the threshold for Faraday waves in a Newtonian fluid is fixed by viscosity. For the inviscid case the threshold is identically zero. For finite viscosity the threshold increases with viscosity [14]. Second, the amplitude of the waves depends on the distance above the threshold. Given these characteristics, it is plausible that the threshold for the Faraday instability in WMS is determined by a dynamical process in which the shear generated

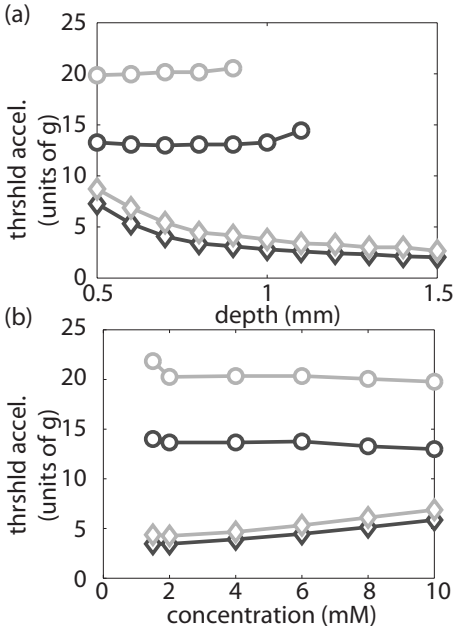

FIG. 5. Threshold acceleration as a function of (a) depth and (b) concentration for frequencies $f=80$ (dark) and $f=120$ Hz (light). The diamonds and circles denote the threshold for Faraday waves and strip waves, respectively. For the varying depth measurements the concentration was 4 mM and for the varying concentration measurements the depth was 0.75 mm. We exclusively used equimolar solutions, and thus the concentration refers to both the concentrations of CTAB and NaSal.

by waves lowers the viscosity thus increasing the distance above threshold.

From the above scenario we expect the onset of Faraday waves, i.e., the transition from the flat state to the corrugated state, to be discontinuous. Consider the threshold for some zero shear-rate viscosity (0.20 Stokes in our system). Since the fluid is initially motionless, Faraday waves will first appear when the acceleration crosses this critical value. But the waves generate shear causing the viscosity to decrease because the fluid is shear thinning. The decreased viscosity increases the apparent distance of the system above threshold, resulting in waves of greater amplitude. Higher amplitude waves cause yet more shear, further lowering the viscosity. This feedback loop will continue to amplify the waves until the viscosity reaches a minimum. In our case, the latter would occur at the crossover from the shear-thinning I to the shear-thickening regime. Moreover, we expect a similar process will cause a discontinuity at the crossover point between the shear-thickening and shear-thinning II regime.

We examined these scenarios with numerical experiments with a nonlinear variant of the Mathieu equation. The Mathieu equation emerges naturally from the linear stability analysis of the inviscid Faraday problem and describes the amplitudes of the modes [15]. While the numerical analysis of Kumar and Tuckerman [16] provides an exact description of the threshold, the Mathieu equation with an *ad hoc* damping term has nonetheless proved useful for describing the threshold and the near-threshold amplitude of the waves [17,18].

We began with the equation derived by Cerda and Tirapegui [19] in which the damping term includes dissipation from the bulk and from the interaction of the surface waves with the bottom of the container,

$$\ddot{\xi}_k + 2\nu k^2 \frac{C_1(kh)}{2C_2(kh)}\dot{\xi}_k + \frac{1}{C_2(kh)}[\omega_k^2 + ak \tanh kh \cos(\Omega t)]\xi_k = 0, \tag{1}$$

where ξ_k is the amplitude of the kth mode surface wave, k and ω_k are its wave number and angular frequency, Ω is the driving frequency, h is the layer depth, and ν is the kinematic viscosity. The dissipation coefficients C_1 and C_2 are given in [19],

$$C_1(s) = \frac{2\tanh s(\cosh 2s + 2s^2 + 1)}{\sinh 2s - 2s}, \tag{2}$$

$$C_2(s) = \frac{\tanh[3\cosh^2 s(\sinh 2s - 2s - 4s^3/3) + s^2(\sinh 2s - 2s)]}{(\sinh 2s - 2s)^2} \tag{3}$$

and the relation between k and ω_k is the usual $\omega_k^2 = (gk + \sigma k^3/\rho)\tanh kh$.

We assume that the most unstable mode $k=\kappa$ corresponds to the resonance condition $\omega_\kappa = \Omega/2$, which is strictly correct in the limit $a \to 0$. Introducing $y = \xi_\kappa/\ell$ and nonlinear detuning by replacing y with $\sin y$ yields

$$\ddot{y} + 2\nu(\dot{y})\kappa^2 \frac{C_1(\kappa h)}{2C_2(\kappa h)}\dot{y} + \frac{1}{C_2(\kappa h)}[\omega_\kappa^2 + a\kappa \tanh(\kappa h)\cos(2\omega_\kappa t)]\sin y = 0, \quad (4)$$

where ν depends on the instantaneous value of $\dot{y}$. A nonlinear term is needed to prevent the oscillatory solutions from diverging [20]. The parameter ℓ is needed for dimensional consistency and reflects the length scale at which nonlinear effects become important. The most likely candidates for this quantity are the fluid depth ($\sim 0.7-2$ mm) or the boundary layer thickness ($\sqrt{2\nu/\omega_\kappa} \sim 180-360$ μm).

We incorporate the viscous response of WMS by allowing the kinematic viscosity to vary as function of the instantaneous shear rate as measured for a 4 mM WMS (shown in Fig. 3). We parameterized the measured viscosity with a piecewise continuous set of linear segments as shown in Fig. 3. The relation between $\dot{y}$ and the shear rate $\dot{\gamma}$ follows from an energy argument [21]. The rate of energy density dissipation is $\rho\nu(C_1/C_2)\dot{y}^2$ in our model and $2\rho\nu\dot{\gamma}^2$ from continuum theory. Hence,

$$\dot{\gamma} = \sqrt{\frac{C_1(kh)}{2C_2(kh)}} k\ell\dot{y}. \quad (5)$$

The numerical results are insensitive to the value of ℓ for $\ell \gtrsim 10^{-2}$ cm; for smaller values the transition to higher amplitudes can be delayed (see below). For our calculations $\ell = 1$ cm. We investigated various forms of nonlinearities (e.g., $y+ay^3$ with $a=\pm 1$, or $\pm 1/6$) before settling on $\sin y$ in Eq. (4). The results are independent of this choice. All calculations, unless noted otherwise, used initial conditions $y(0)=10^{-4}$ and $y'(0)=0$.

Numerical integration of Eq. (4) gave either decaying, periodic, or chaotic solutions depending on the magnitude of the driving parameter a. Chaotic solutions arise from the nonlinearity introduced by the sine term, and are not physical relevant for our system as they are present whether the viscosity is Newtonian or non-Newtonian. For the periodic solutions we took half the peak-to-peak distance as the measure of the amplitude. In order to isolate the effect of introducing a shear-dependent viscosity we began our numerical experiments with a Newtonian viscosity model, and introduced successively a shear-thinning regime, a shear-thickening regime, and a final shear-thinning regime which plateaued to a shear-rate independent viscosity. Below we report our results at each stage of this process. The results of our computations are summarized in Fig. 6. The corresponding viscosity model is shown in the insets.

Figure 6(a) shows the amplitude as a function of acceleration for a constant kinematic viscosity equal of 0.12 St. Our model by construction reproduces the well-known behavior of Faraday waves in a Newtonian fluid. At a critical acceleration a_c there is a supercritical transition to oscillations, and above the transition the amplitude increases as the square root of the distance above threshold $(a-a_c)/a_c$. In our calculations the transition occurs at an acceleration of 9.5 g. At even higher accelerations ($a \approx 20$ g) the model produces chaotic solutions. Chaos in the Mathieu equation is well established; for our particular application in which we are investigating the impact of the dissipative term on the solutions, we ignore these chaotic solutions because they arise irrespective of the rheology whenever the drive is sufficiently large.

For a shear-thinning rheology our model also produces a transition to an oscillating state, but unlike when the viscosity is constant the transition is discontinuous as shown by the (red) circles in Fig. 6(b). For this rheology the viscosity was 0.2 St at zero shear rate, thinned to 0.12 St by 8 s^{-1}, and was shear-rate independent thereafter. As argued above, we expect a discontinuous transition because the shearing due to the waves lowers the viscosity which in turn allows the waves to grow. We observe in our calculation that the transition to Faraday waves is subcritical with the marginal stability point set by the zero shear-rate viscosity. For accelerations above the marginal stability point, the quiescent state loses stability to a finite amplitude limit cycle. The limit cycle branch can be traced back to a saddle-nose bifurcation that manifests when the acceleration crosses the threshold for the plateau viscosity $\nu_\infty = 0.12$ St. This is illustrated by the similarity of the curve in Fig. 6(a) and the (green) squares in Fig. 6(b) which are the results of the computation with $y(0)$ set to a large value 10^{-2}. Thus, once the transition occurs, the fluid behaves as though its viscosity were ν_∞.

Introducing a shear-thickening regime following the shear-thinning regime does not qualitatively change the observed states. The shear-thinning/shear-thickening rheology was implemented as shown in Fig. 6(c) inset. The numerical solutions are similar to those found with a shear-thinning rheology, except that the solution is trapped by the steep rise in viscosity after the shear-thinning regime and the amplitude remains small.

Lastly, we implemented the second shear-thinning regime in WMS. We terminated the shear-thinning II regime with a plateau of 0.08 St for shear rates above 400 s^{-1} because otherwise the viscosity would continue to fall and ultimately cross zero. Figure 6(d) shows the amplitude versus acceleration for the full rheology of the 4 mM WMS. These data shows a second discontinuity.

The state after the second discontinuity is chaotic, and thus required further analysis to determine if the transition is due to the nonlinearity of the Mathieu equation or to the shear-dependence of the viscosity. The inset in Fig. 6(d) shows the measured viscosity of a 4 mM WMS. The dashed line shows a continuation scheme given by the ν_2 model in Table I in which the viscosity is assumed to be constant above some shear rate. The computed final state for this viscosity model is oscillatory. Moreover, the acceleration threshold for the transition to the oscillatory state is identical to that found for the full rheology. Thus, we concluded that the transition for the measured rheology is due to the shear-rate dependence.

IV. DISCUSSION

Our model shows that given the two shear-thinning regimes observed in the viscous response, we should expect to see two transitions. Furthermore, our model shows that the

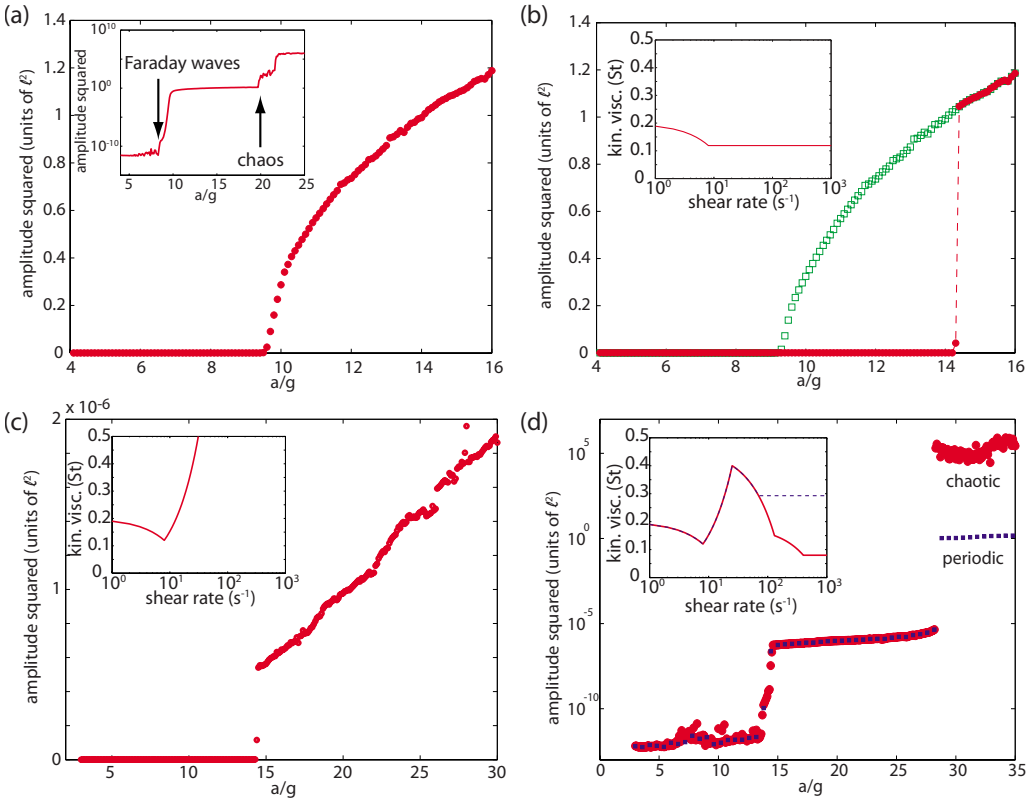

FIG. 6. (Color online) Amplitude squared versus acceleration calculated from Eq. (4) at $f=120$ Hz for (a) Newtonian fluid and (b)–(d) various non-Newtonian rheologies shown in the insets. (a) Shows a $\sqrt{a-a_c}$ rise characteristic of Faraday waves in a simple fluid with $\nu=0.12$ St. Inset shows the amplitude at higher acceleration. Note the transition to chaos at $a\approx 20$ g. (b) Solid (red) circles show a discontinuous transition to Faraday waves for a shear-thinning rheology. Open (green) squares show the transition to Faraday waves for a sufficiently large perturbation. Note that the Faraday wave branch traces the same curve as shown in Newtonian case (a). (c) Discontinuous transition to Faraday waves for a shear thinning followed by a shear-thickening rheology. (d) Transitions produced by the full rheology of a 4 mM WMS (red filled circles) shown in inset and for a rheology which plateaus at high shear rate (solid blue squares) as shown by the dashed curve in inset.

first of these transitions is from a constant time-independent solution to a oscillatory solution with finite amplitude, and that the second transition is from an oscillatory solution to a large amplitude oscillatory. The model thus qualitative reproduces the sequence of transitions observed in our experiments.

Figure 7 shows the phase boundaries measured experimentally (open symbols), calculated from our model (filled

TABLE I. Piecewise linear models of viscosity. Viscosity for shear rates not listed is given by linear interpolation between nearest two values.

$\dot{\gamma}$ (s^{-1})	ν_1 (St)	ν_2 (St)	ν_3 (St)
0	0.2	0.2	0.07
8	0.12	0.12	0.04
25	0.4	0.4	0.3
70	n/a	0.29	n/a
130	0.15	0.15	0.15
400	0.08	0.15	0.08
∞	0.08	0.15	0.08

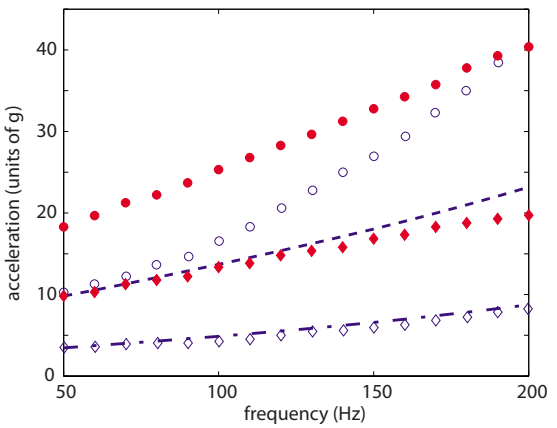

FIG. 7. (Color online) Phase diagram as a function of acceleration and frequency from model (filled symbols) and observation (unfilled symbols). Diamonds correspond to the transition to Faraday waves and the circles correspond to the transition to strip waves, as in Fig. 4. The dashed curves are the acceleration threshold values for the Faraday instability calculated by linear stability analysis for the full hydrodynamic theory [16] with $\nu=0.2$ St (—) and $\nu=0.08$ St (–·).

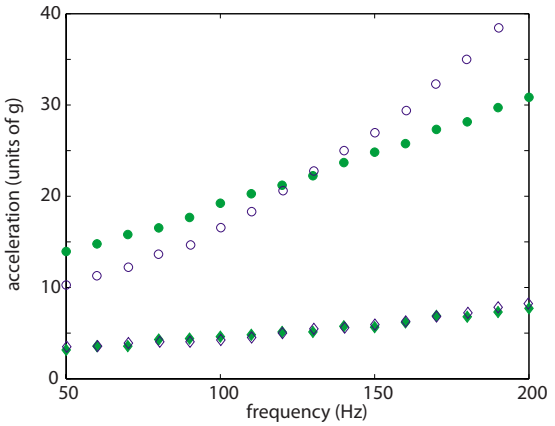

FIG. 8. (Color online) Phase diagram as a function of acceleration and frequency. Results of model calculated with ν_3 in Table I shown with filled symbols and observations shown with unfilled symbols. The symbols are same as in Fig. 4

symbols) with $\nu=\nu_1$, and calculated from the full hydrodynamic analysis for a Newtonian fluid by Kumar and Tuckerman [16]. The Faraday threshold from the model and the stability analysis are in good agreement, but these differ substantially from the measured values. If we use $\nu=0.08$ St, instead of the 0.2 St measured in steady shear, the stability calculation reproduces the experimentally observed boundary. This indicates that the discrepancy is due to the value of viscosity input to the model rather than to a problem with the model itself.

It is unsurprising that there is a quantitative discrepancy between the measured and calculated phase boundaries. The viscosity in the model comes from a spatially homogenous, time-independent measurement. In contrast, the waves on the fluid excite specific spatial and temporal scales and thus probe the fluid's response on scales different than the steady measurements. Our model can be used to back out the response of the fluid, but given the *ad hoc* nature of our extensions to Eq. (1) we expect the results to be only approximate. Figure 8 shows the results of tuning the viscosity to values that reproduce the measured boundaries reasonable well. To accomplish the latter we used the ν_3 model in Table I. In principle, the agreement can be improved by employing a frequency-dependent viscosity, but we will not pursue this avenue any further because the main intent of our model is to demonstrate that the multiple shear-thinning regimes can account for the observed transitions.

The original motivation for these experiments was to test the hypothesis that shear-thickening is responsible for the solitary structures observed in particulate suspensions [4,5,10]. Since WMS shear-thicken we expected to observe solitary structures in our experiments. Although we do observe solitary structures in WMS, the mechanism to which we attribute these is unlikely to apply to particulate suspensions. The mechanism we propose for strips waves relies on the transition of the fluid from shear-thickening to shear thinning. First, while there is some evidence for a shear-thinning phase following shear-thickening in particulate suspensions (e.g., [22]), the observation remains contentious. Second, even if there is such a transition it occurs at shear rates much higher than the onset of persistent holes [5].

Our study leaves a number of open questions. We are puzzled by the absence of an induction time. In the steady-state measurements of viscosity there is always an initial transient period before the viscosity reaches its asymptotic value. The conventional wisdom is that during this period there is a buildup of the shear-induced-structures that determine the stress response of the material. This initial period typically lasts hundreds of seconds. Yet, in our experiments we see strip waves develop within in seconds (see Fig. 1). Thus, whatever microstructural transition is occurring in WMS to produce strip waves, the buildup time is several order of magnitude faster than we expected given the steady shear measurements.

Yet another feature of our observations we cannot explain is the striplike form of strip waves. Our model, which simply describes the amplitude of a homogenous field, does not include spatial variations. Nonetheless, one possible answer suggested by the model is that the transverse localization is partly due to volume conservation. Our model shows that large amplitudes are to be expected in fluids with a shear-thickening to shear-thinning transition with increasing shear rate, but there is insufficient fluid to produce large amplitude waves everywhere. Thus, large amplitude waves can only exist in some fraction of the containers area roughly equal to the ratio of fluid depth to the amplitude of the waves.

V. CONCLUSION

Our experiments show that dilute CTAB-Nasal wormlike micellar solutions vibrated in a Faraday system display two transitions. The first is a garden-variety transition to Faraday waves. The second is a new instability in which the fluid localizes into strips of large amplitude waves. Through a model based on the Mathieu equation we can identify that the second transition arises from a local maximum in the shear-rate dependent viscosity. Waves in parametrically driven systems are only possible when energy pumped into the system is sufficient to balance dissipation. Thus, viscosity dissipation constrains the amplitude of the waves. When the viscosity decreases as a result of the wave motion, as it does in our wormlike micellar system, there is the potential for instability. The success of our model, in reproducing the experimentally measured phase boundaries and the change in amplitude at the transition, suggests that this instability scenario is unfolding in the creation of the strip wave state. We expect that the same instabilities will occur in other shear-thickening dilute wormlike micellar solutions.

ACKNOWLEDGMENT

This material is based upon work supported by the National Science Foundation under Grant No. 0932600.

[1] M. Faraday, Philos. Trans. R. Soc. London **121**, 299 (1831).
[2] C. Wagner, H. W. Muller, and K. Knorr, Phys. Rev. Lett. **83**, 308 (1999).
[3] F. Raynal, S. Kumar, and S. Fauve, Eur. Phys. J. B **9**, 175 (1999).
[4] O. Lioubashevski, H. Arbell, and J. Fineberg, Phys. Rev. Lett. **76**, 3959 (1996).
[5] F. S. Merkt, R. D. Deegan, D. I. Goldman, E. C. Rericha, and H. L. Swinney, Phys. Rev. Lett. **92**, 184501 (2004).
[6] P. Ballesta and S. Manneville, J. Non-Newtonian Fluid Mech. **147**, 23 (2007).
[7] P. Ballesta and S. Manneville, EPL **76**, 429 (2006).
[8] P. Ballesta and S. Manneville, Phys. Rev. E **71**, 026308 (2005).
[9] H. Shiba, J. E. Ruppert-Felsot, Y. Takahashi, Y. Murayama, Q. Ouyang, and M. Sano, Phys. Rev. Lett. **98**, 044501 (2007).
[10] H. Ebata, S. Tatsumi, and M. Sano, Phys. Rev. E **79**, 066308 (2009).
[11] S. Lerouge and J.-F. Berret, e-print arXiv:0910.1854.
[12] P. Boltenhagen, Y. Hu, E. F. Matthys, and D. J. Pine, EPL **38**, 389 (1997).
[13] Y. T. Hu, S. Q. Wang, and A. M. Jamieson, J. Rheol. **37**, 531 (1993).
[14] K. Kumar, Proc. R. Soc. London, Ser. A **452**, 1113 (1996).
[15] T. B. Benjamin and F. Ursell, Proc. R. Soc. London, Ser. A **225**, 505 (1954).
[16] K. Kumar and L. S. Tuckerman, J. Fluid Mech. **279**, 49 (1994).
[17] O. Lioubashevski, J. Fineberg, and L. S. Tuckerman, Phys. Rev. E **55**, R3832 (1997).
[18] A. V. Kityk, K. Knorr, H. W. Muller, and C. Wagner, EPL **65**, 857 (2004).
[19] E. A. Cerda and E. L. Tirapegui, J. Fluid Mech. **368**, 195 (1998).
[20] S. Fauve, in *Hydrodynamics and Nonlinear Instabilities*, edited by C. Godreche and P. Manneville (Cambridge University Press, Cambridge, England, 1998).
[21] L. D. Landau and E. M. Lifshitz, *Fluid Mechanics* (Elsevier, New York, 1987).
[22] H. M. Laun, R. Bung, S. Hess, W. Loose, O. Hess, K. Hahn, E. Hadicke, R. Hingmann, F. Schmidt, and P. Lindner, J. Rheol. **36**, 743 (1992).